Advances in Science and Technology Research Journal

Advances in Science and Technology Research Journal, 2025, 19(6), 362–372
https://doi.org/10.12913/22998624/202961
ISSN 2299-8624, License CC-BY 4.0

Received: 2025.02.06
Accepted: 2025.04.15
Published: 2025.05.01

Assessment of the potential application of medium-carbon steels subjected to the process of surface induction hardening for constant velocity joint components

Krzysztof Włoch[1,2], Sylwia Wencel[2*], Paweł Wieczorek[2], Piotr Szablewski[3]

[1] Neapco Europe Sp. z o.o., ul. Kaliska 72, 46-320 Praszka, Poland
[2] Faculty of Production Engineering and Materials Technology, Czestochowa University of Technology, Aleja Armii Krajowej 19, 42-201 Czestochowa, Poland
[3] Institute of Mechanical Engineering, University of Kalisz, ul. Nowy Świat 4, 62-800 Kalisz, Poland
* Corresponding author's e-mail: sylwia.wencel@pcz.pl

ABSTRACT

The paper presents the results of an analysis on the feasibility of using low-alloy medium-carbon steels for the induction surface hardening process in the production of internal components for constant-velocity joints, as an alternative to low-carbon steel components subjected to carburizing. The research results concerning the microstructure analysis, including the stereological characteristics of the ferritic phase of selected grades of low-alloy medium-carbon steels, were used to select the optimal grade recommended for the induction surface hardening process. The next stage of the work involved designing a new structure for the internal components of the constant-velocity joint. The design process took into account requirements related to strength, durability, and wear resistance of the joint components. To verify the correctness of the designed structure, a finite element analysis (CAE) was conducted to assess the distribution of maximum stresses acting on the joint. The CAE analysis allowed for the evaluation of stress distribution in the joint components under operational loads and the identification of any potential critical areas. The CAE analysis results confirmed the correctness of the designed structure and the appropriateness of the chosen material for manufacturing the constant-velocity joint components.

Keywords: medium-carbon steels, induction surface hardening, constant-velocity joint components.

INTRODUCTION

Modern cars, regardless of the type of drive (front-wheel drive, rear-wheel drive, all-wheel drive – Fig. 1), use constant-velocity joints to transfer torque from the engine to the wheels. These joints enable smooth and efficient operation of the drivetrain even at high steering angles and under varying loads [1–3].

From the perspective of design and application, there are several types of constant-velocity joints, each differing in construction, operational characteristics, and areas of use [4]. Each type of joint is designed to meet specific requirements of drivetrain systems, ensuring optimal torque transfer as well as compensation for suspension movements and working angles [5]. Choosing the right joint is crucial for ensuring reliability, efficiency, and driving comfort. Typical spherical constant-velocity joints include: Rzeppa joints, which are known for their high efficiency under large angles; Cross Groove joints, which have smaller working angles but offer excellent noise damping and vibration minimization while compensating for axial suspension movements; and Double Offset joints, which are more prone to generating vibrations and noise but allow for operation at larger angles compared to Cross Groove joints, providing longer axial compensation, making them ideal for off-road vehicles and those with large suspension travel and working angles (Fig. 2) [6, 7]. One of the key components of constant-velocity joints is the inner race, which plays a fundamental

Figure 1. Types of automotive drivetrains (FWD – front-wheel drive, RWD – rear-wheel drive, AWD – all-wheel drive)

Figure 2. Main types of constant-velocity joints (a) Rzeppa, (b) cross groove, (c) double offset

role in ensuring their durability and reliability [8, 9]. Its design and material properties are crucial for the entire drivetrain system. The inner race of a constant-velocity joint must not only be wear-resistant but also capable of handling large dynamic loads encountered during vehicle operation. To meet these requirements, the inner races of constant-velocity joints undergo a carburizing process. As a result, a hard, wear-resistant surface is created that effectively resists wear, which is essential for ensuring the long service life of the constant-velocity joint.

The inner races are typically made from low-carbon steel. Their geometry is precisely designed to allow free movement of the joint while maintaining structural stiffness. The inner race features grooves where the joint's balls operate, enabling smooth torque transmission with inimal loss of transmitted force (Fig. 3) [10].

The accuracy of the inner race manufacturing directly affects the smoothness of movement and efficiency of torque transfer. Improperly made inner races can lead to undesirable vibrations, noise, and accelerated wear of the joint. Therefore, it is crucial that the inner race is produced with the highest precision using advanced machining technologies [11–13].

The heat treatment process via batch carburizing of many components in the form of races, located in different parts of the batch, causes significant and uneven surface deformations that require additional "hard" mechanical machining

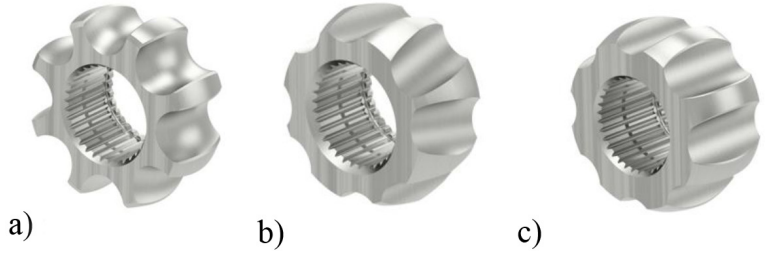

Figure 3. Example inner races of a spherical constant-velocity joint. (a) for Rzeppa joint, (b) for cross groove joint, (c) for double offset joint

(after the heat treatment process) for precise finishing of these surfaces. Additionally, the carburizing process affects the entire carburized component, leading to significant deformations of the splines, which are used to connect the carburized components to the intermediate shaft connecting the outer and inner joints during the final assembly of the drive shaft. Significant spline deformations cause problems with achieving the correct pressing forces for the press-fit connection, which are typically defined within a specific range of minimum and maximum pressing forces intended to eliminate potential issues related to generating noise by the drive shaft (known as NVH = noise, vibration, & harshness).

The paper presents the results of an analysis on the feasibility of using low-alloy medium-carbon steels for the induction hardening process in the production of internal components of constant-velocity joints (inner races) as an alternative to low-carbon steel components subjected to carburizing. The proposed heat treatment method, utilizing induction hardening for internal components of constant-velocity joints, is expected to enable a continuous and more cost-effective production process while significantly reducing surface deformations. This method eliminates the need for heat treatment in the spline area, ensuring a very precise press-fit connection with the intermediate shaft, thus minimizing defects related to the pressing forces in the production process [14–17]. This is particularly important for electric vehicles, which have more stringent requirements for noise reduction compared to internal combustion engines, as there are no damping factors to mitigate potential noise generated by the drive shaft.

By changing the technology for producing the inner races, constant-velocity joints can meet the demands of modern drivetrain systems, ensuring smooth and reliable torque transfer to the wheels even under the most challenging operating conditions.

The article presents the results of preliminary studies on the chemical composition and microstructure of selected low-alloy medium-carbon steels to determine their suitability for use in the production of inner races for constant-velocity joints. The results of the analysis were used to select the optimal steel grade for use in the induction surface hardening process, considering chemical composition, microstructure, mechanical properties, and production costs. The next phase of the work involved designing a new structure for the internal components of the constant-velocity joint. The design process took into account the requirements for strength, durability, and wear resistance of the joint components. To verify the accuracy of the designed structure, a finite element analysis (CAE) was performed to assess the distribution of maximum stresses on the joint. The CAE analysis allowed for the evaluation of stress distribution in the joint components under operational loads and the identification of potential critical areas. The CAE analysis results confirmed the correctness of the designed structure and the appropriateness of the chosen material for manufacturing the constant-velocity joint components.

ANALYSIS OF THE CHEMICAL COMPOSITION AND MICROSTRUCTURE

In the technology for producing inner races for constant-velocity joints, low-carbon steels are used for carburizing. In the proposed technology discussed in the article, which involves replacing carburizing with induction hardening, medium-carbon steels are planned to be used. Therefore, an analysis of the chemical composition and microstructure of selected low-alloy medium-carbon steels was conducted to determine their suitability for use in the production of inner races for constant-velocity joints, with induction hardening as the surface hardening method. The materials chosen for the study were rods that underwent hot deformation in three steel grades: C50, C45, and 37MnB4. The chemical compositions of the studied steel grades are presented in Table 1.

Microstructure analysis

To assess the suitability of the different steel grades for the induction hardening process, an evaluation of the microstructure of the rods in the delivery condition was conducted using optical microscopy. This evaluation was performed on longitudinal and transverse sections of the rods with an Axiovert 25 optical microscope. The microstructure analysis was carried out in the areas where the heat treatment via induction hardening will be performed.

For the selected hot-rolled bars, the depth of the decarburized layer during the hot rolling process was determined first. Figure 4 shows an example measurement of the decarburized zone. The depth of the decarburized layer for all the

Table 1. Chemical composition of the analyzed steel grades, %wt

Steel grade	Chemical composition, %										
	C	Si	Mn	P	S	Cu	Cr	Ni	Mo	Al	Ti
C50	0.50	0.26	0.77	0.017	0.013	0.24	0.21	0.15	0.04	0.03	-
C45	0.48	0.28	0.74	0.01	0.009	0.21	0.30	0.17	0.04	0.005	-
37MnB4	0.40	0.28	0.89	0.012	0.006	0.21	0.18	0.14	0.03	0.031	0.034

bars selected for testing was significantly smaller than the material allowance that was provided for the preliminary mechanical processing before the induction hardening process. The images of the microstructures are presented in Figures 5÷7.

In each of the analyzed materials, the structure consists of a mixture of ferrite and pearlite. However, for subsequent induction hardening, the most favorable structure will be one characterized by uniformity in grain size and an even distribution of ferrite, with the highest degree of dispersion.

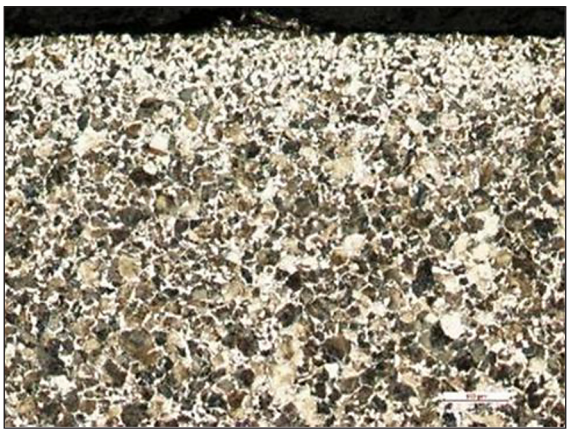

Figure 4. Microstructure of the surface layer of a hot-rolled bar made of C50 steel with the visible decarburized layer

The analysis indicates that these expectations are best met by the material made from C50 steel. Both the transverse and longitudinal sections show fine-dispersed ferrite grains located at the boundaries of pearlite grains (Fig. 5a and 5b). This structural state ensures a uniform carbon content in the austenite during the induction heating of the material. Uniform austenite protects the hardened component from cracking during the induction hardening process.

The structure shown in Figure 6a exhibits significant banding of ferrite, while Figure 6b reveals ferrite grains with a needle-like structure embedded within the pearlite grains. This structural effect adversely affects the induction hardening process, leading to cracking during the intensive cooling of the material.

Figures 7a and 7b display a very coarse pearlite grain structure. The proportion of pearlitic phase is significantly higher compared to the ferritic phase in relation to the other analyzed steel grades. Such a structure necessitates a longer austenitizing time during induction heating to achieve uniform austenite, which is associated with grain growth and, consequently, lower mechanical properties of the heat-treated steel.

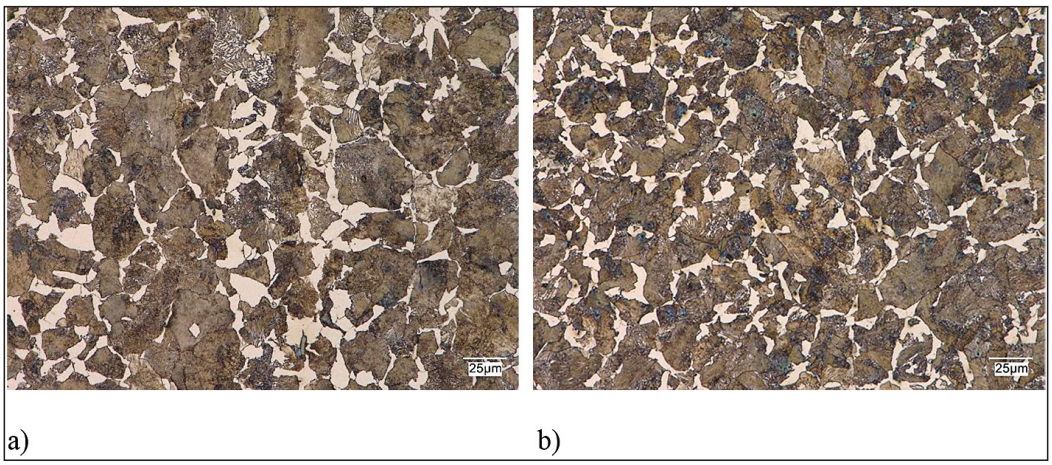

Figure 5. Microstructure of C50 steel: (a) longitudinal section in the rolling direction of the rod, (b) transverse section to the rolling direction of the rod, etched with Nital

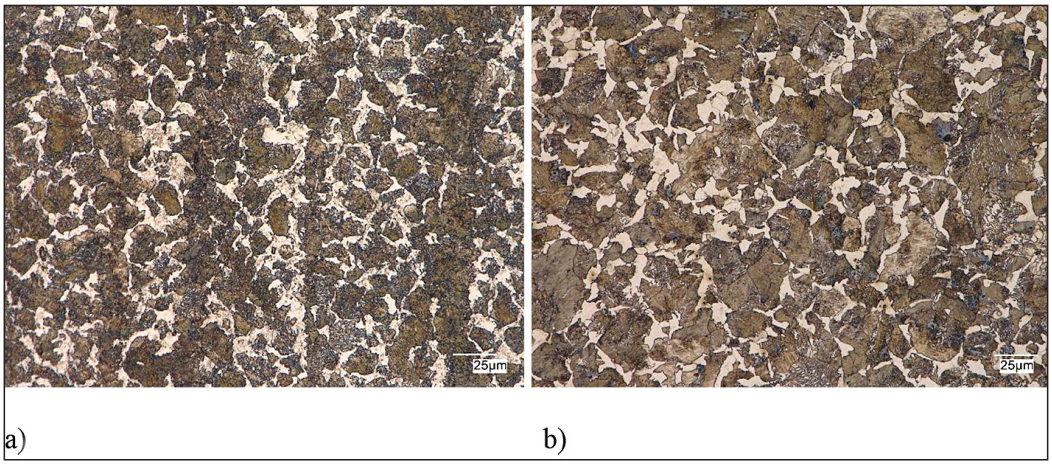

Figure 6. Microstructure of C45 steel: (a) longitudinal section in the rolling direction of the rod, (b) transverse section to the rolling direction of the rod, etched with Nital

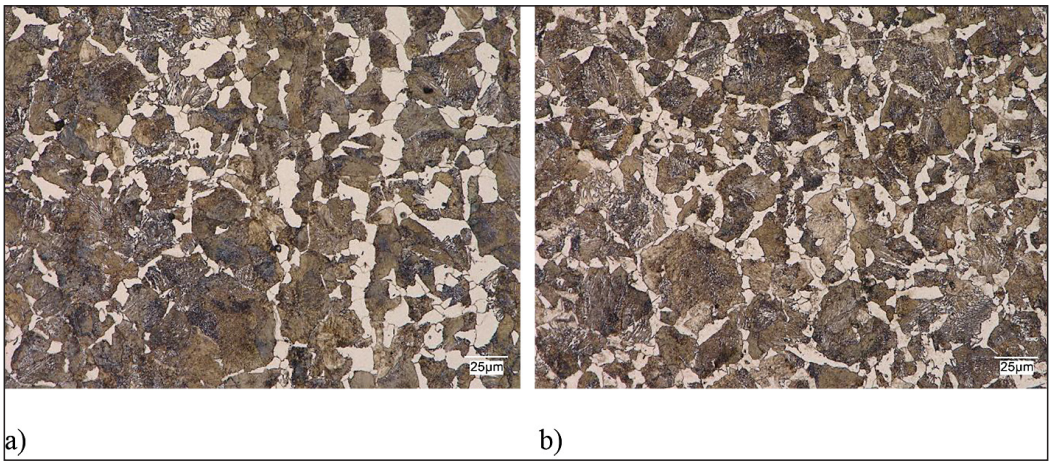

Figure 7. Microstructure of 37MnB4 steel: (a) longitudinal section in the rolling direction of the rod, (b) transverse section to the rolling direction of the rod, etched with Nital

Analysis of ferrite grain size

To evaluate the suitability of various steel grades for the induction hardening process, a stereological analysis of ferrite grain size was conducted for longitudinal and transverse sections using a computer-based image analyzer. The images were obtained using Keyence VHX-7000 digital microscope. At the beginning shadow effect and was corrected. In the next step noise filter was applied. After that pictures were binarized and prepared to computation by threshold setting, fill holes, opening, closing and separation filters. Built-in image analyzer was used. This analyzer utilize planimetric and linear methods according ISO 643 Standard.

The analysis of the ferrite grain size for the selected bars was conducted in areas where subsequent induction hardening is planned. The distance was determined based on the shape of the structural element and the diameter of the bar (the locations of the ferrite grain size measurements are shown in Figure 8). The results of the analysis are presented in Table 2.

The study conducted an analysis of the ferritic phase present in the structures of the examined steels C45, C50, and 37MnB4 from a stereological perspective. The average ferrite grain area, as well as the average maximum and minimum ferrite grain diameters, were determined. The investigations were carried out on metallographic sections taken in the direction of rolling and in the direction perpendicular to rolling.

The planned induction hardening must achieve maximum uniformity of austenite in terms of carbon content during heating. This process is facilitated by greater dispersion of the ferritic phase, which is associated with a shorter carbon diffusion

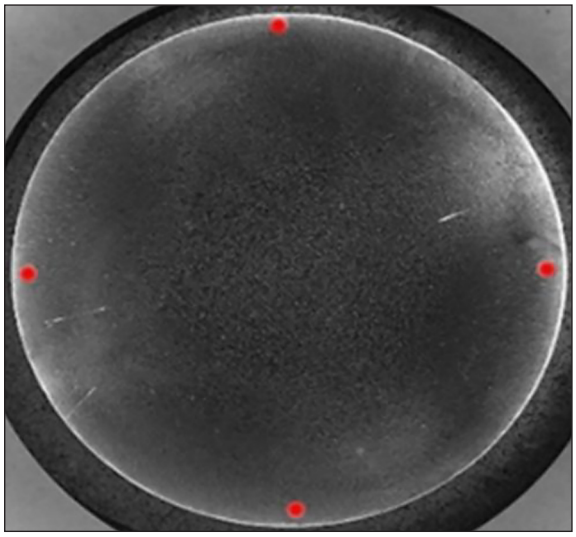

Figure 8. Cross-section of a hot-rolled bar with marked areas for ferrite grain size measurements

path following the austenitic transformation. The studies showed that the average ferrite grain areas for 37MnB4 and C45 steels are similar, both in longitudinal and transverse sections relative to the rolling direction of the rods. In contrast, the C50 steel exhibits distinctly smaller ferrite grain sizes, as evidenced by both the average grain area and the average maximum and minimum ferrite grain diameters.

Achieving uniform ferrite grain size is particularly important in the induction hardening process. Statistical analysis of the obtained values for average grain area, maximum average diameter, and minimum average diameter of ferrite grains showed that the C50 steel has the most uniform ferrite grain size. The standard deviation of the average ferrite grain area is twice as small as that for C45 steel. Table 2 also includes a parameter representing the percentage of grains with an area up to 15 μm². This parameter indicates the level of ferrite grain dispersion in the examined steel grades. In this case, the C50 steel shows the highest percentage of grains with an area up to 15 μm², which is 50% of all ferrite grains analyzed in the structure. The analysis revealed that 37MnB4 steel has a structure with the largest ferrite grains, with only 30% of grains having an area up to 15 μm² in the longitudinal section and 44% in the transverse section.

Table 2. Results of the stereological analysis of ferrite grain size for longitudinal and transverse sections of the examined steel grades

Parameter	37MnB4 transverse section	37MnB4 longitudinal section	C45 transverse section	C45 longitudinal section	C50 transverse section	C50 longitudinal section
Average area, μm²	25.2	37.3	25.2	33.3	18.5	21.1
Maximum average diameter, μm	8.1	9.9	8.6	9.1	7.1	7.2
Minimum average diameter, μm	4.3	5.3	4.5	4.7	4	4
Standard deviation of the average area	22.26	33.43	25.21	45.27	12.71	21.05
Standard deviation of the maximum average diameter	3.77	4.63	4.66	5.87	2.74	3.65
Standard deviation of the minimum average diameter	2.14	2.71	2.69	3.3	1.52	2.25
Percentage of grains up to 15 μm²	44	30	45	42	49	50

Table 3. Ranking of functional parameters for different types of joints

Parameter	Efficiency	Weight	Axial compensation	Operating angle	Vibrations/Noise	Rating
	> 99.5%	< 1.5 kg	Min 25 mm	4°	Vibration Amplitude < 50mm/s²	
CGi (Cross groove)	+	+	+	+	++	13
FRi (Rzeppa)	0	++	+	+	++	12
DOi (Double offset)	0	++	++	++	0	8
Parameter weight	3	2	1	1	3	-

CALCULATIONS AND DESIGN OF NEW COMPONENTS FOR MEDIUM-CARBON STEEL GRADE C50

Due to the many possible design variations of joints used in automotive drives, a comprehensive approach was employed to identify the best possible type of joint that meets the base requirements most effectively. For this purpose, a comparison of possible designs along with their evaluation was prepared. The ranking of functional parameters for the various types of joints is presented in Table 3.

Based on the comparative analysis of key functional parameters, the Cross Groove (CGi) joint type was selected for further research and development. The Cross Groove joint enables the transfer of torque through the driveshaft at varying angles while maintaining a constant rotational speed, regardless of the operating angle. It also minimizes vibrations and noise, which is a crucial factor for the use of this type of joint in electric vehicles. Additionally, due to its design, this type of joint provides axial compensation within the driveshaft, accommodating suspension movements and wheel steering.

This joint type can be configured with various specific "interfaces" used by different car manufacturers (OEMs), such as stem, flange, or face spline constructions. The tracks where the joint balls operate are aligned at the same angle in both the external joint housing and the internal hub. A cage is positioned between the external and internal housings to keep the balls in the correct working plane at a constant speed, regardless of the angle.

As part of the design tasks, which included accounting for all design assumptions and defined main functional parameters, detailed calculations were performed for the joint's construction. This included calculations for the internal hub's spline, the external track diameter, ball diameter, effective pitch circle diameter (PCD), and the maximum diameter of the intermediate shaft to achieve the maximum joint angle. The calculations also confirmed that the design goals were met concerning the maximum allowable stresses for the joint's individual components, especially the internal hub, given its manufacture from C50 steel. Figure 9 shows the model of the designed joint.

For this purpose, spreadsheets from Neapco's proprietary "know-how" were used, correlated with the mechanical properties of C50 steel subjected to induction hardening, based on equations found in the literature [18].

After designing and modeling the joint construction, a comparative analysis was conducted with a competitive solution available on the market, including a direct comparison of the mass of the designed joint with the competing solution. The results of this analysis are presented in Table 4.

As part of the research, a cross-groove (CGi) joint design was developed that is competitive with the best similar solutions currently available on the market in terms of weight.

ANALYSIS OF THE NEW DESIGN CONSIDERING STRESS ANALYSIS USING FINITE ELEMENT METHOD (CAE)

To verify the correctness of the designed structure, a stress distribution analysis for the joint was carried out using the finite element method (CAE). The CAE analysis allowed for the assessment of stress distribution in the joint components under operational loads and the identification of potential critical areas. The analysis was conducted not only for the internal raceway but for all joint components, as it is important to consider the mutual interactions of the cooperating parts. The design assumptions required that the allowable values for max. principal stresses of 2350 N/mm² and max. hertzian stresses of 4200 N/mm² not be exceeded.

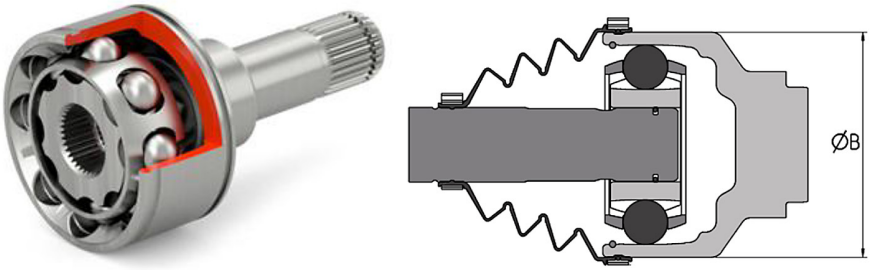

Figure 9. Model of the designed CGi2700 joint. Diameter B = 85.2 mm

Table 4. Comparative summary of the mass of the designed joint construction compared to the competing solution

Element of the joint	Masa, kg	
	CGi2700	Competitor's joint
Outer housing (raceway)	1.015	1.115
Inner hub (raceway)	0.263	0.165
Basket	0.066	0.085
Balls (8 pcs)	0.128	0.160
Retaining ring	0.006	-
Complete joint	1.478	1.525

Consideration of dynamic effects

The analysis primarily focused on static and quasi-static load cases. However, in practical applications, the joint operates under dynamic conditions, where additional factors such as material fatigue, variable operating temperatures, and the influence of the lubricant's friction coefficient play a crucial role.

- material fatigue: fatigue effects were not directly incorporated into the current static stress analysis, but they are indirectly considered through material selection and surface treatment. The induction-hardened C50 steel, with a case hardness of 58–63 HRC and a hardened layer depth of at least 0.8 mm (with a minimum of 50 HRC at this depth), ensures improved fatigue resistance. Future work will focus on fatigue simulations to predict component lifespan under cyclic loading conditions.
- variable operating temperatures: the analysis was performed under room temperature conditions, assuming a homogeneous material response. Temperature fluctuations in real-world applications can affect material properties and stress distribution. Future studies will include thermal simulations to assess temperature-dependent effects.
- lubricant and friction effects: the influence of lubrication on frictional forces was not explicitly modeled in the current study. The CV joint typically operates with high-performance grease, which impacts stress distribution through changes in frictional contact. Planned research includes tribological simulations to evaluate friction-induced stress variations.

Boundary conditions and load selection

The CGi2700 8Ball joint variant was analyzed under multiple loading conditions to simulate realistic operational stresses. The analysis included the external raceway, cage, balls, internal raceway, splines, and pin. The joint model was created using Catia V5 software (Fig. 10).

The geometric model was implemented into Abaqus Standard 6.14-1, and preprocessing was carried out using HyperMesh v13.0. A nonlinear static stress analysis was performed in Abaqus Standard 6.14-1.

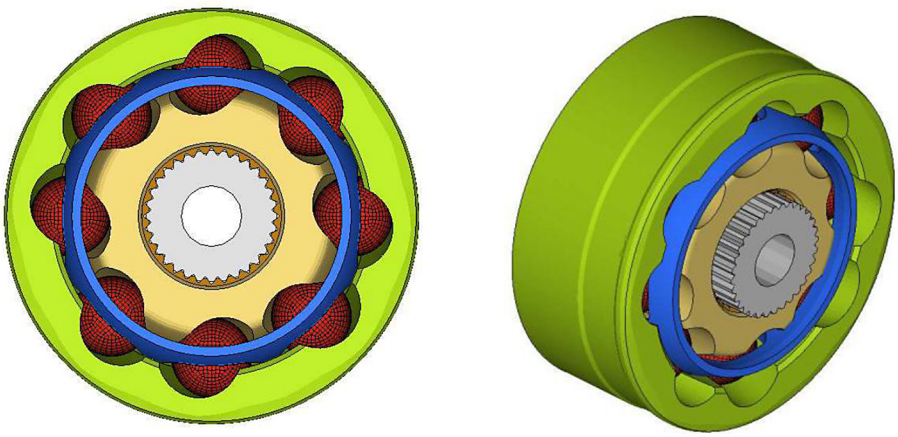

Figure 10. Joint model implemented for numerical simulation

The material properties used in the simulation were:

- Young's modulus: 205,000 N/mm²,
- Density: 7.85 kg/dm³,
- Poisson's ratio: 0.29,
- Material: C50 steel.

Boundary conditions

The external raceway was fixed in all global translation directions at the spline area to simulate the constraint imposed by the driveline structure. The pin of the shaft was fixed at an angle of 20 degrees in local translation and rotation directions X' and Z' to replicate the real-life joint articulation constraints. A torque of 1650 Nm was applied around the local Y' axis on the pin to replicate real operating loads. To ensure accuracy, the loading conditions were selected based on experimental data and design requirements. The applied loads were derived from standard operational scenarios, including static torsion, quasi-static torsion, and dynamometer strength tests. Figure 11 illustrates the applied boundary conditions and loads in the simulation. The results of the maximum principal stresses and Hertzian stresses for all joint components, along with the test conditions, are presented in Table 5. The maximum stress distributions are shown in Figures 12–14.

The internal criteria for maximum allowable stresses for all analyzed loading conditions have been met. The calculated Hertzian stress of 3480 MPa is within the acceptable limit of 4200 MPa, and the calculated principal stress of 1989 MPa is within the acceptable limit of 2350 MPa, ensuring the joint's strength and durability under the given load conditions. For the inner race, the C50 material is considered suitable for induction hardening, which is also assumed for the outer race. The surface hardness achieved by induction hardening is in the range of 58–63 HRC, with a case depth of the hardened layer having a minimum of 50 HRC at 0.8 mm. This material selection and heat

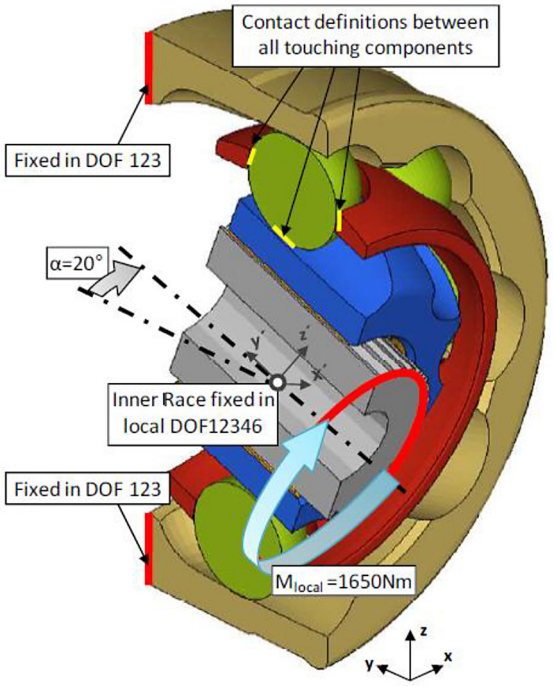

Figure 11. Boundary conditions and loads applied in the simulation

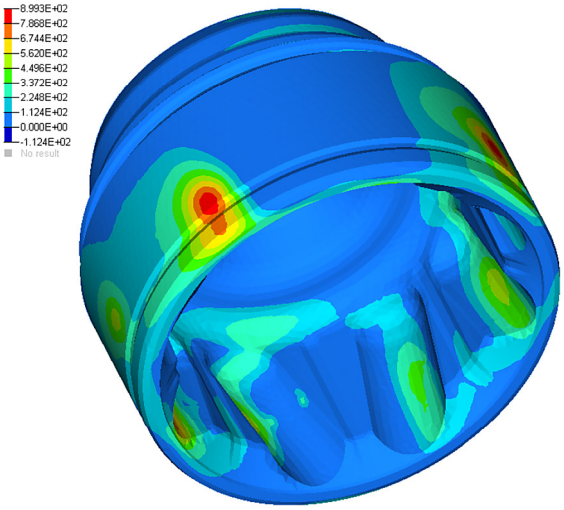

Figure 12. Locations of maximum stresses on the outer housing (Raceway)

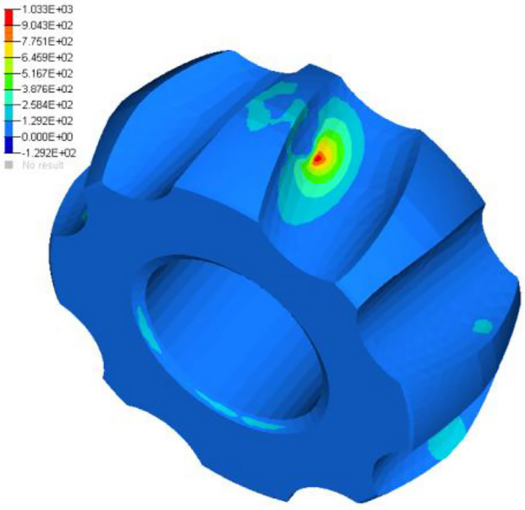

Figure 13. Locations of maximum stresses on the inner hub (Raceway)

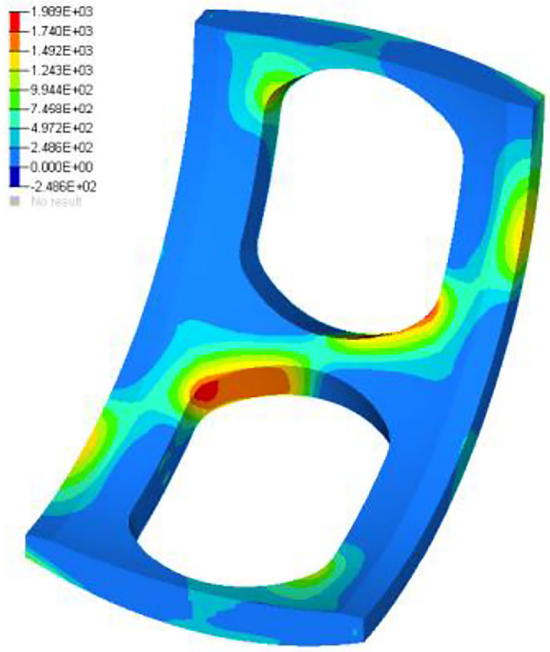

Figure 14. Locations of maximum stresses on the cage

treatment process provide adequate resistance to wear and fatigue, further enhancing the durability of the CV joint.

CONCLUSIONS

The metallographic analysis revealed that the structures observed on longitudinal sections for C45 and 37MnB4 steels exhibit significant banding of the ferritic phase, which is an undesirable property in relation to the planned surface heat treatment by induction hardening. This banding phenomenon will lead to variations in the carbon saturation of the austenite during the induction hardening process, resulting in expected material cracks during the intense cooling phase following the induction hardening process.

The metallographic analysis for C50 steel showed only a slight degree of banding in the ferrite grains on the longitudinal section and a uniform distribution of the ferritic phase in the transverse section. Therefore, C50 steel is the optimal material among those analyzed in the study for use in the surface induction hardening process.

The stereological analysis of the ferritic phase in the studied steel grades indicates that C50 steel is the recommended material for the induction hardening process. This is due to its smallest average ferrite grain size, highest degree of grain uniformity, and the largest percentage of ferrite grains in the analyzed structure.

The newly designed CGi (cross groove) joint was competitive compared to the best-known similar solutions currently available on the market in terms of weight. Numerical simulations confirmed that the internal criteria for maximum allowable stresses were met for all analyzed load conditions and all components of the joint developed during the research.

Acknowledgments

Work funded by the Ministry of Education and Science as part of the 6th edition of implementation doctorates No. DWD/7/0174/2023.

REFERENCES

1. Micknass W., Popiol R., Sprenger A.: Clutches, gearboxes, drive shafts, and half shafts. WKiŁ 2009.
2. Bedros J., Katarzynski S.: Diagnostics of passenger cars. WKiŁ, Warsaw 1993.
3. Wiśniewski K.: Passenger cars - technical descriptions and regulatory data. WKiŁ, Warsaw1995.
4. Hillier, V.A.W.; Coombes, P. Fundamentals of Motor Vehicle Technology, 4th ed.; Nelson Thornes: Cheltenham, UK, 1991.
5. Wagner, E.; Cooney, C. Universal Joint and Driveshaft Design Manual; Society of Automotive Engineers: Warrendale, PA, USA, 1979.
6. Serveto, S.; Mariot, J.P.; Diaby, M. Modelling and measuring the axial force generated by tripod joint of automotive drive-shaft. Multibody Syst. Dyn. 2007, 19, 209–226.
7. Serveto, S.; Mariot, J.P.; Diaby, M. Secondary torque in automotive drive shaft ball joints: Influence of geometry and friction. Proc. Inst. Mech. Eng. Part K-J. Multi-Body Dyn. 2008, 222, 215–227.
8. Jo, G.H.; Kim, S.H.; Kim, D.W.; Chu, C.N. Estimation of generated axial force considering rolling-sliding friction in tripod-type constant velocity joint. Tribol. Trans. 2018, 61, 889–900.
9. Kim, S.H.; Kim, D.H.; Jo, G.H. An Experimental and Numerical Study on Reduction of Generated Axial Force. Appl. Sci. 2021, 11, 8836. https://doi.org/10.3390/app11198836
10. Santonocito, P. and Pennestri, E., A parametric study of the dynamics of the shudderless tripode joint, in Proceedings of DETC 2000/MECH-14079, Baltimore, USA, September 10–13, 2000, 1–6.
11. Mabie, H.H., Constant velocity joints, Machine Design, May 1948, 101–105.

12. Durum, M.M., Kinematic properties of tripode joints, ASME Journal of Engineering for Industry, 1975, 708–713.
13. Akbil, E. and Lee, T.W., On the motion characteristics of tripode joints. Part 1, General case, Part 2, Applications, ASME Journal of Mechanisms, Transmissions and Automation in Design 106, 1984, 228–234 and 235-241.
14. Ismail R, Prasetyo DI, Tauviqirrahman M, Yohana E, Bayuseno AP. Induction Hardening of Carbon Steel Material: The Effect of Specimen Diameter. AMR 2014;911:210–4. https://doi.org/10.4028/www.scientific.net/amr.911.210
15. Coupard D, Palin-luc T, Bristiel P. Residual stresses in surface induction hardening of steels: comparison between experiment and simulation. Mater Sci Eng A 2008; 487: 328–339.
16. Srivastava A., Jain A., Rajput S., Singh H.O., Kandpal B.C., Yadav M., Varshney S., Johri N., Structural and FEM analysis of heat treatment effects on mild steel, Materials Today: Proceedings, Volume 46, Part 20, 2021, Pages 11064-11071, https://doi.org/10.1016/j.matpr.2021.02.204
17. Garois, S., Daoud, M. & Chinesta, F. Explaining hardness modeling with XAI of C45 steel spur-gear induction hardening. Int J Mater Form 16, 57 (2023). https://doi.org/10.1007/s12289-023-01780-1
18. Seherr-Thoss H.Cr., Schmelz F., Aucktor E., Universal Joints and Driveshafts, Analysis, Designs, Applications, Second, enlarged edition, Translated by J. A.Tipper and S. J.Hill, Springer-Verlag Berlin Heidelberg 2006.